# Thermoelectric properties of *p*-type $CoSb_3$ nanocomposites with dispersed $CoSb_3$ nanoparticles

L. Yang,[1] H. H. Hng,[1,a)] D. Li,[1] Q. Y. Yan,[1] J. Ma,[1] T. J. Zhu,[2] X. B. Zhao,[2] and H. Huang[3]
[1]*School of Materials Science and Engineering, Nanyang Technological University, Singapore 639798, Singapore*
[2]*Department of Materials Science and Engineering, State Key Laboratory of Silicon Materials, Zhejiang University, Hangzhou 310027, China*
[3]*Sensors and Actuators Laboratory, School of Electrical and Electronic Engineering, Nanyang Technological University, Singapore 639798, Singapore*

(Received 2 April 2009; accepted 24 May 2009; published online 7 July 2009)

$CoSb_3$ nanocomposites with different contents of $CoSb_3$ nanoparticles were prepared by mixing nanosized $CoSb_3$ particles obtained via polyol method and micron-sized particles obtained via solid state reaction. X-ray diffractometer and field emission scanning electron microscope were used to characterize the prepared products. The thermoelectric properties of the nanocomposites with different amounts of nanoparticles as dispersants were measured from room temperature to around 500 °C. Due to the grain boundaries scattering, the lattice thermal conductivity was observed to decrease as the amount of nanoparticles increased. The electrical properties were also improved by the addition of nanoparticles. The *ZT* value of the nanocomposites with 10 wt % of nanoparticles was nearly doubled that of the sample without any nanoparticles. © *2009 American Institute of Physics*. [DOI: 10.1063/1.3157202]

## I. INTRODUCTION

Thermoelectric (TE) devices can reliably convert heat into useful electricity, and have no noise or vibration as there are no mechanical moving parts.[1] They are also small in size and light in weight. The heat can come from the sun, or can be waste heat generated by a variety of sources including power plants, chemical plants, or automobiles. The basic idea is to use thermoelectric modules to convert part of the waste heat back into useful electricity, thereby improving the overall energy efficiency. However, the main problem with today's TE devices is poor efficiency. Therefore, the development of better performance TE materials is of great importance.[2]

The efficiency of a TE material at a particular temperature $T$, is determined by the dimensionless figure of merit $ZT$, where $Z=\alpha^2/\rho\kappa$, and $\alpha$ is the Seebeck coefficient, $\rho$ is the electrical resistivity, and $\kappa$ is the total thermal conductivity. The total thermal conductivity is often approximately described as $\kappa=\kappa_l+\kappa_e$, where $\kappa_l$ is the heat conducted by phonons (lattice vibration) and $\kappa_e$ is the heat conducted by mobile electrons.[3] Over the past 10 years or so, intensive research effort worldwide has identified several novel TE materials that, with further development, could bring about the breakthrough and open up new horizons for a widespread use of thermoelectricity. Among these materials, skutterudites lead the way for application in the intermediate temperature range.[4]

Of the different types of skutterudites, $CoSb_3$-based materials have attracted the greatest attention because of their large Seebeck coefficient and high electrical conductivity.[5] However, their lattice thermal conductivity is relatively high as compared to other TE materials. Hence, many research approaches have been considered to decrease the lattice thermal conductivity and improve the *ZT*. One promising method is through nanostructuring. The decrease in the grain size of the material lead to a drastic increase in the density of grain boundaries, which brings about a significant reduction in the thermal conductivity, and hence improve the value of *ZT*.[3,5,6] Theoretical predictions have shown that nanostructuring reduces the thermal conductivity by the selective scattering of phonons as a result of a much higher density of grain boundaries.[6] According to Rayleigh scattering regime, the scattering cross section varies as $\sigma \propto b^6/\lambda^4$, where $b$ is the size of the scattering particle and $\lambda$ is the phonon wavelength.[7,8] The mid- and long-wavelength phonons are greatly scattered by the dense grain boundaries. However, the decreased grain size reduces the electrical conductivity at the same time. Hence, a nanocomposite approach in which nanoscaled structures are incorporated into the matrix of a conventional bulk TE material is explored in order to strike a balance between nanostructures and bulk materials. Many kinds of TE nanocomposites have been reported, such as PbTe nanocomposites with coated nanostructures on the surface of the bulk,[9] $Bi_2Te_3$ nanotube-containing nanocomposites,[10] and also $CoSb_3$ nanocomposites containing $ZrO_2$, $Yb_2O_3$, $FeSb_2$, and $CoSb_3$.[11–13]

In this work, our original motivation is to reduce the thermal conductivity and at the same time maintain the good electrical properties by preparing $CoSb_3$ composites with different amount of $CoSb_3$ nanoparticles as dispersants. From the results, it was found that the difference in electrical properties between the dispersants and matrix can have a positive effect on the electrical properties of the nanocomposites. Hence, the effects of nanoparticles on the nanocomposite

a)Author to whom correspondence should be addressed. Electronic mail: ashhhng@ntu.edu.sg.

 

thermoelectrical properties: electrical resistivity, Seebeck coefficient, thermal conductivity, and the overall *ZT* value, will be presented and discussed in this work.

## II. EXPERIMENTAL PROCEDURES

Sample preparation includes (1) synthesis of nanosized $CoSb_3$ particles by a modified polyol process; (2) solid state reaction to synthesize micron-sized $CoSb_3$ particles; (3) mixing of the nanosized dispersants and micron-sized matrix; and (4) synthesis of the final $CoSb_3$ nanocomposite samples using hot press.

A modified polyol process was used to synthesize pure nanosized $CoSb_3$ particles, and the detailed experimental procedures have been presented elsewhere.[14] The nanosized $CoSb_3$ particles prepared by polyol method are *p*-type semiconductors due to the excess Sb in the chemical reaction. Hence, 0.25 at. % excess of Sb shots was added in order to obtain *p*-type micron-sized $CoSb_3$. The bulk materials were prepared by solid state reaction. Co powders (99.9%) and Sb shots (99%) were used as the starting materials. Powder mixtures were loaded into a quartz ampoule in an argon-atmosphere glovebox. The ampoules were sealed under the vacuum of $10^{-3}$ Pa, and then heated up to 800 °C at a rate of 1 °C/min and kept at 800 °C for 84 h.

The final composite pellets were prepared by first mixing the micron-sized particles and with various amount of nanosized particles (0, 10, 20, 30, and 100 wt %) by horizontal ball milling, and then hot pressed at 500 °C for 120 min under vacuum with a uniaxial pressure of approximately 100 MPa.

Phase identification was performed through XRD analysis using a Shimadzu 6000 x-ray diffractometer. The morphology of the samples was determined by observing the fractured cross section of the sample using a field emission scanning electron microscope (FESEM) (JEOL JSM6340F).

The thermal diffusivity $D$ and the specific heat capacity $C_p$ were measured under argon atmosphere using laser flash (NETZSCH LFA 457). Specific heat capacity $C_p$ was determined using the ratio method by comparing the temperature rise of the sample to the temperature rise of a standard sample of known specific heat tested under the same conditions. The density $\rho$ was measured by Archimedes method at room temperature. Thermal conductivity $\kappa$ was calculated using the equation: $\kappa = D \times \rho \times C_p$.

The Seebeck coefficient and electrical resistivity were determined by a standard four probe method using ULVAC ZEM-3 in a He atmosphere.

## III. RESULTS AND DISCUSSION

Figure 1 shows the XRD pattern of the hot pressed pellets obtained from nanocomposites with various amount of nanosized particles. It should be noted that there are additional diffraction peaks in the patterns which correspond to the Al sample holder. The samples are named nano-*XX*%, where *XX* indicates the weight percentage of nanosized particles in the sample, and the sample bulk means there is no nanosized particles added.

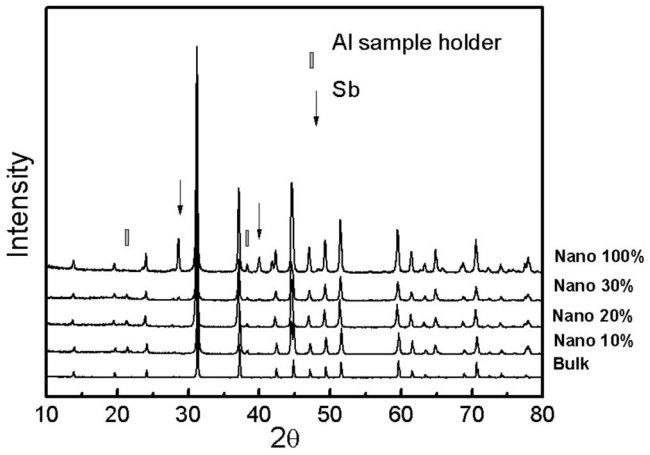


FIG. 1. XRD pattern of the sample pellets with various amount of nanosized particles prepared by hot press.

After the hot pressing process, it is observed that additional diffraction peaks corresponding to the Sb phase were detected for pellets containing the $CoSb_3$ nanosized particles. The intensity of the Sb peaks was also observed to increase with increasing amount of $CoSb_3$ nanosized particles in the nanocomposites. It was also noted that there is no excess Sb phase in the bulk sample, indicating that the excess Sb does not come from the micron-sized particles. Hence, the excess Sb must come from the $CoSb_3$ nanosized particles. A possible reason for the detection of the Sb phase in the hot pressed pellets is that the synthesized nanosized Sb-rich $CoSb_3$ phase was metastable, and during the hot pressing process, the excess Sb in the Sb-rich $CoSb_3$ metastable phase would rather exist as the elemental Sb phase, instead of existing in the $CoSb_3$ phase.

Figure 2(a) shows a typical FESEM image of the fracture surface of sample bulk indicating that the sample consists of only micron-sized grains. Figures 2(b)–2(d) correspond to sample nano-10%, nano-20%, and nano-30%, indicating that the samples contain both nanosized and micron-sized grains. They have similar microstructures except for the amount of nanosized particles distributed among the micron-sized matrix. Most of these nanosized particles exist as clusters residing mainly between the micron-sized particles. Figure 2(e) reveals the morphology of hot pressed sample nano-100% without micron-sized powders. Compared to the as-synthesized powders obtained through polyol method, the particle size has increased from about 30 to about 50 nm.

The electrical resistivity plotted as a function of temperature for all the samples are shown in Fig. 3. The resistivity of the sample bulk and nano-100% are observed to decrease with temperature over the whole temperature range measured, which indicates a semiconductor behavior. However, for samples nano-10%, nano-20%, and nano-30% (shown in the inset figure), the resistivity increases with temperature up to 150 °C, which is indicative of a metallic behavior. With further increase in temperature, the resistivities of these samples decrease as temperature increases. It is noted that by adding only 10 wt % percent of nanosized particles, the resistivity decreases significantly as compared

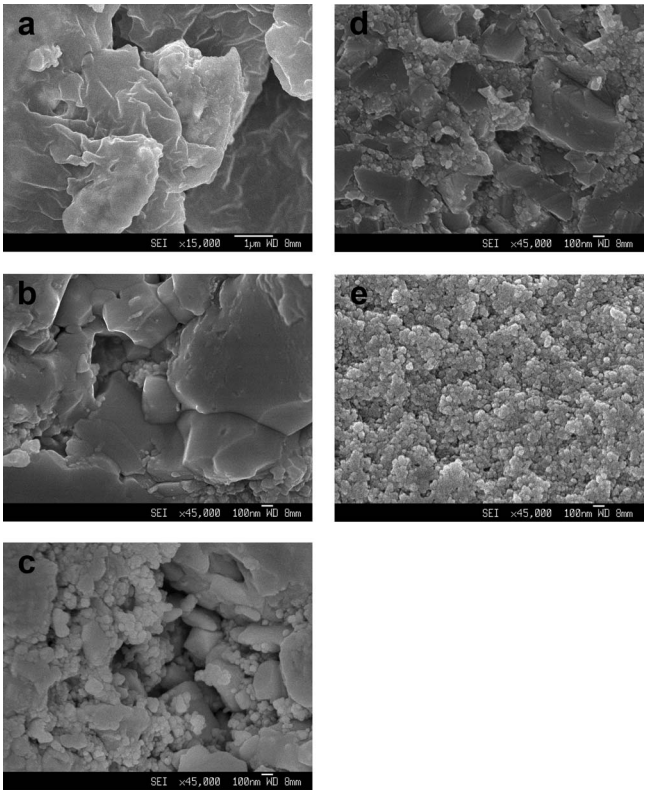


FIG. 2. The typical FESEM images of the fracture surface of bulk (a), nano-10% (b), nano-20% (c), nano-30% (d), and nano-100% (e).

to the sample bulk by one order of magnitude. This phenomenon indicates that the carrier concentration of the nanosized particles is much higher than that of the micron-sized matrix. In order to verify this, Hall effect measurements were carried out to determine the carrier concentration at room temperature. The dependence of the carrier concentration versus the weight percentage of nanosized particles is shown in Fig. 4. All the samples are of $p$ type which is in a good agreement with the positive Seebeck coefficients (the results will be presented later) obtained. The carrier concentration of sample bulk is about $10^{17}$ $cm^{-3}$ and the carrier concentrations of the samples increase as the amount of nanosized

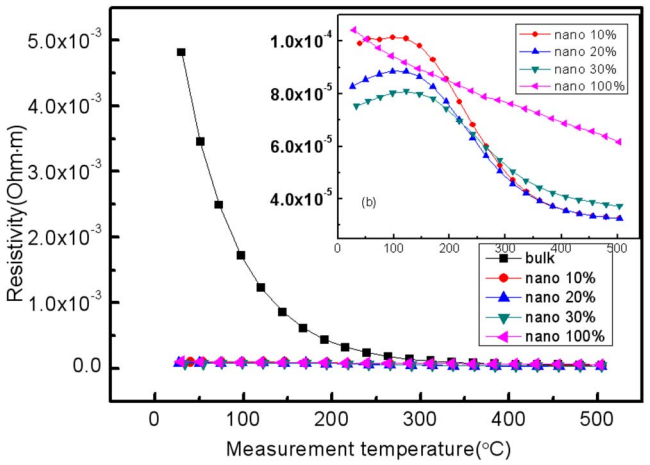


FIG. 3. (Color online) Temperature dependences of resistivity of the samples with various amount of nanosized particles. The inset is a magnified plot of samples nano-10%, nano-20%, nano-30%, and nano-100%.

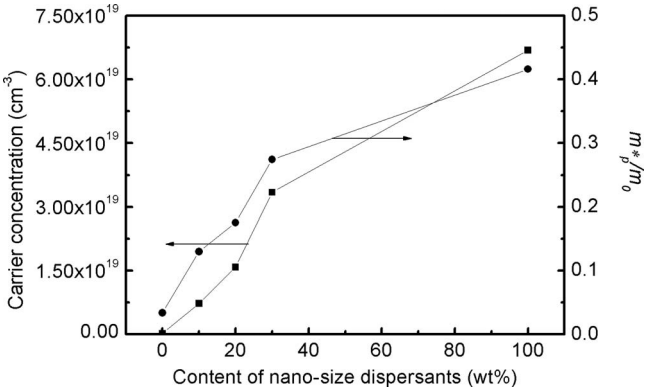


FIG. 4. The dependence of the carrier concentration and effective carrier mass vs the weight percentage of nanoparticles at room temperature for the samples with various amount of nanosized particles.

particles increases. The change in the carrier concentration and electrical properties may be related to the excess Sb phase arising from the nanosized particles, as earlier mentioned in the XRD results. The effect of excess elemental Sb on carrier concentration has also been reported by Liu *et al.*[15]

Within the measured temperature range, sample bulk and nano-100% exhibit semiconductor behavior. The plots of $\log(\rho)$ versus inverse temperature for these two samples are presented in Fig. 5(a). The solid line is fitted to the equation:[15]

$$\rho(T) = \rho_0 \exp(E_g/2k_BT), \tag{1}$$

where $\rho_0$ is a constant, $k_B$ is Boltzmann constant, and $E_g$ is the band gap. For sample bulk, $E_g$ was determined to be 0.43 eV, which is close to the reported band gap of $CoSb_3$ (0.5 eV).[5] This $E_g$ level is likely due to the intrinsic band gap. For sample nano-100%, $E_g$ of 0.04 eV was obtained. This is much smaller than the band gap of $CoSb_3$ indicating that $E_g$ of nano-100% arises from a shallow acceptor level, which is much easier to be activated and hence causing an increase in the carrier concentration. This is in agreement with the Hall measurement results.

In order to understand the conduction mechanism of the nanocomposites samples (nano-10%, nano-20%, and nano-30%), the temperature range can be divided into two parts. From room temperature to 150 °C, the samples show metallic behavior as indicated from the resistivity results. For temperatures above 150 °C, it is proposed that small polaron hopping conduction (SPHC) model can be applied:

$$\rho(T) = \frac{1}{ne\mu} = \frac{T}{C}\exp\left(\frac{E_p}{k_BT}\right), \tag{2}$$

where $n$ is the carrier concentration, $e$ is the electrical charge of carrier, $\mu$ is the carrier mobility, $C$ is a constant, $E_p$ is the activation energy of polaron hopping, and $k_B$ is the Boltzmann constant. By plotting $\ln(\rho/T)$ versus $1/T$ for samples nano-10%, nano-20%, and nano-30% [Figs. 5(b)–5(d)], it is found that the temperature dependence of the resistivity in the semiconductorlike temperature range of these nanocomposites fits well to the SPHC model. The activation energy $E_p$ in the semiconductor temperature range can be determined by performing a linear fit of the experimental data.

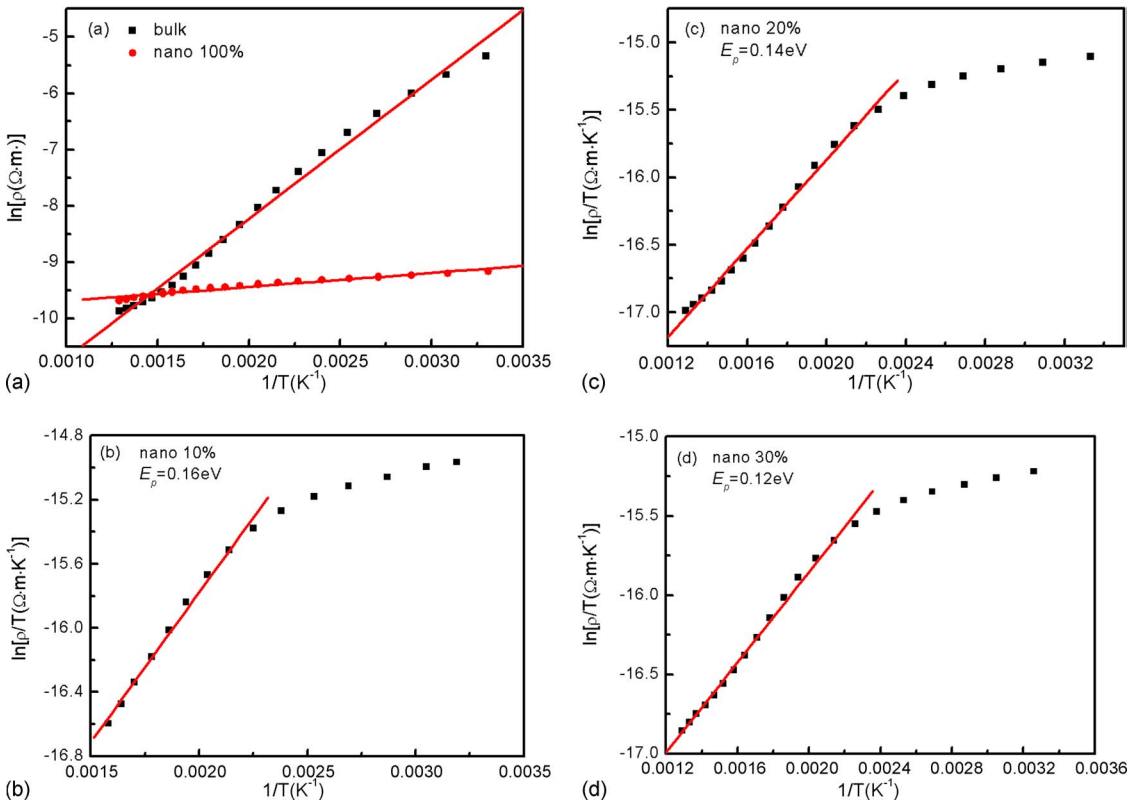


FIG. 5. (Color online) Plots of $\ln(\rho)$ vs $1/T$ of sample bulk and nano-100% (a) and plots of $\ln(\rho/T)$ vs $1/T$ of sample nano-10% (b), nano-20%, (c) and nano-30% (d).

The $E_p$ data obtained for the nanocomposite samples with different amount of nanosized particles are presented in the respective plots. These values are smaller than the band gap of $CoSb_3$, indicating that the electrical conductivity is mainly due to small polaron hopping conduction, and the intrinsic activation does not occur within the temperature range measured. It is also noted that the activation energy $E_p$ decreases with increasing amount of nanosized particles. The decrease in the activation energies indicates that the transport of the polarons becomes easier with increasing amount of the nanosized particles which is consistent with Hall measurement results that the nanosized particles have higher carrier concentration. Meanwhile, the increasing amount of nanosized particles can also cause more distortions on the sites neighboring the polaron, and such distortions aid in the motion of the carriers. It should be mentioned that the resistivity of sample nano-100% is higher than these three nanocomposite samples. In the sample nano-100%, the carriers are scattered by the dense grain boundaries. This decreases the mobility of the carriers, and hence leads to a higher electrical resistivity obtained in this sample.

Figure 6 shows the Seebeck coefficient as a function of temperature with different amount of nanosized particles. The positive values indicate that the samples are $p$ type. The Seebeck coefficient of the samples investigated decrease as the amount of nanosized particles is increased.

The carrier effective mass $m_p^*$ was estimated using the Seebeck coefficient and Hall carrier concentration data by assuming a single parabolic band model with acoustic phonon scattering as a predominant carrier scattering mechanism. In this model,[16] the Seebeck coefficient $\alpha$ can be expressed as follows (our samples are all $p$ type):

$$\alpha_p = \frac{k_B}{e}\left(\frac{2F_1(\eta)}{F_0(\eta)} - \eta\right). \tag{3}$$

The carrier concentration $n$ can be expressed as follows:

$$n_p = 4\pi\left(\frac{2m_p^* k_B T}{h^2}\right)^{3/2} F_{1/2}(\eta), \tag{4}$$

where $n_p$ is the carrier concentration, $m_p^*$ stands for effective mass of the carrier (holes for our samples), $k_B$ is Boltzman's constant, $\eta$ is the reduced Fermi energy, $F_x$ is the Fermi integral of order $x$, and $T$ is the absolute temperature. The

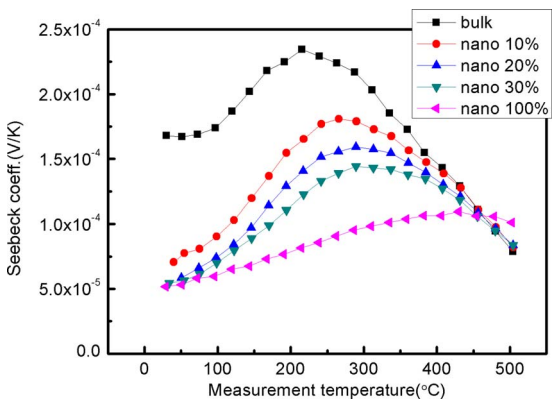


FIG. 6. (Color online) Temperature dependences of Seebeck coefficient of the samples with various amount of nanosized particles.

effective mass of the carriers for all the samples were calculated and plotted against the weight percentage of nanosized particles as shown in Fig. 4. The effective mass for *p*-type materials whose major carriers are holes is smaller than that of *n* type. From the results, one can see that the effective mass increases with increasing amount of nanosized particles dispersants. In general, carrier concentration and effective mass are the two main factors affecting the Seebeck coefficient values. The Seebeck coefficient $\alpha_p$ increases with increasing effective carrier mass $m_p^*$, and decreases with increasing carrier concentration $n_p$. Even though the effective masses increase with increasing amount of nanosized particles dispersants, the Seebeck coefficients of our samples decrease with increasing amount of nanosized particles. Hence, in our samples, carrier concentration has a larger effect than the effective carrier mass on the final Seebeck coefficient. From the Hall effect measurement results, the carrier concentration of nanosized particles is higher than that of the micron-sized matrix, it is reasonable that the Seebeck coefficient decreases with increasing amount of nanosized particles dispersants.

For the sample bulk, the Seebeck coefficient reaches a maximum at about 200 °C. For temperatures above 200 °C, the increasing carrier concentration activated by the intrinsic band gap becomes the dominant factor affecting the Seebeck coefficient, and the Seebeck coefficient decreases. For samples nano-10%, nano-20%, and nano-30%, the Seebeck coefficients reach their highest value at temperatures ranging from 250 to 300 °C. At temperatures above 300 °C, the Seebeck coefficients of these three samples decrease. This decrease is due to the small polaron hopping activation within this temperature range. The increase in the carrier concentration due to small polaron hopping activation leads to a reduction in the Seebeck coefficients. Hence, the results of electrical conductivity and Seebeck coefficient are in good agreement with each other.

Figure 7(a) shows the temperature dependences of total thermal conductivity with different amount of nanosized particle dispersants. The thermal conductivity of a material is the sum of the two contributions, the carrier thermal conductivity and the lattice thermal conductivity. $\kappa=\kappa_c+\kappa_l$, where, $\kappa_c$ and $\kappa_l$ are thermal conductivities, contributed by charge carriers and lattice, respectively. To separate these two effects, the carrier thermal conductivity was estimated using Wiedemann–Franz's law, $\kappa_c=LT/\rho$, where $L$ is the Lorenz number, which is $2.45\times10^{-8}$ $V^2$ $K^{-2}$ for our materials, $\rho$ is the electrical resistivity, and $T$ is the temperature in kelvins. The lattice thermal conductivity $\kappa_l$ for the samples obtained by subtracting $\kappa_c$ from $\kappa$ is shown in Fig. 8(b). As predicted, the nanosized particles dispersants play an important role in reducing the lattice thermal conductivity which is the main contribution to the total thermal conductivity. As the amount of nanosized particles increases, i.e., the grain boundaries increase, the lattice thermal conductivity reduces over the entire temperature range measured. At 50 °C, the lattice thermal conductivity decreases from 8.10 W $m^{-1}$ $K^{-1}$ (sample bulk) to 1.94 W $m^{-1}$ $K^{-1}$ (sample nano-100%).

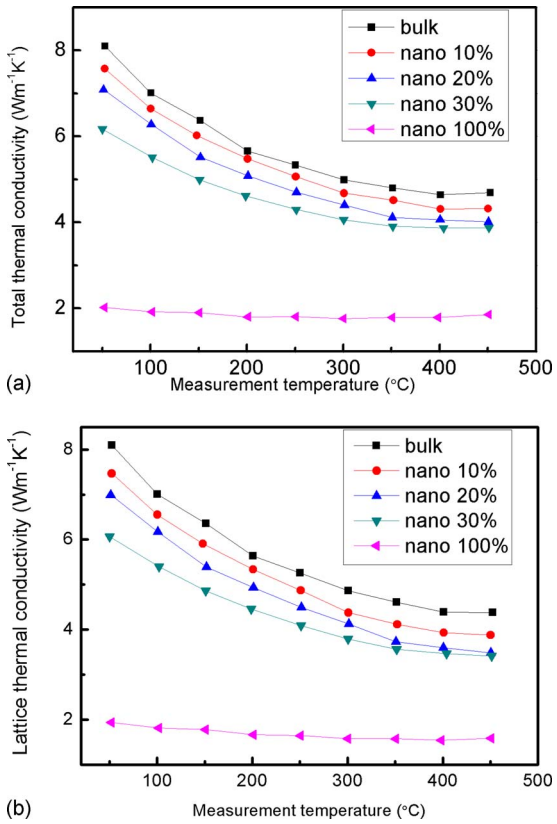


FIG. 7. (Color online) Temperature dependences of total thermal conductivity (a) and lattice thermal conductivity (b) of the samples with various amount of nanosized particles.

The effect of porosity on the thermal conductivity was also estimated using the effective conductivity model which is applied for insulator dispersants,[17]

$$\kappa_0 \approx \frac{\kappa_d}{1-\frac{3f}{2}}, \tag{5}$$

where $\kappa_0$ and $\kappa_d$ are thermal conductivities of the nondispersed and dispersed samples, respectively, and $f$ is the volume fraction of dispersants. To eliminate the effects of porosity on thermal conductivity of our nanocomposite samples, we can consider the pores to be the dispersants in

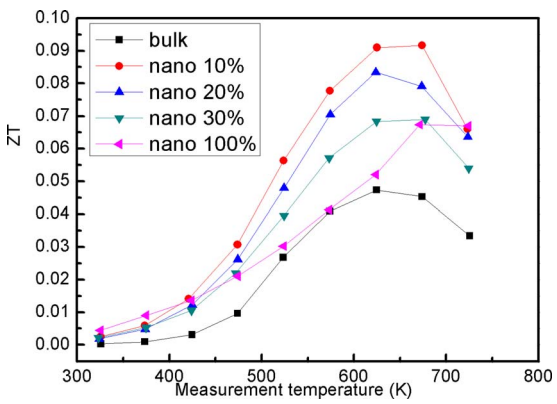


FIG. 8. (Color online) Temperature dependences of dimensionless figure of merit *ZT* value for the samples with various amount of nanosized particles.

TABLE I. The relative density and relationship between $\kappa_0$ and $\kappa_d$ of the samples with various amount of nanosized particles.

| Sample | Relative density | $\kappa_0 \approx \kappa_d/(1-3/2f)$ |
|---|---|---|
| Bulk | 93% | $\kappa_0 \approx 1.12\kappa_d$ |
| Nano-10 wt % | 92% | $\kappa_0 \approx 1.14\kappa_d$ |
| Nano-20 wt % | 92% | $\kappa_0 \approx 1.14\kappa_d$ |
| Nano-30 wt % | 91% | $\kappa_0 \approx 1.16\kappa_d$ |
| Nano-100 wt % | 88% | $\kappa_0 \approx 1.21\kappa_d$ |

the nanocomposites, and $f$ is equal to the porosity which can be expressed as $f=1$-relative density. Hence, by considering the relative density, the relationship between $\kappa_0$ and $\kappa_d$ for our samples can be listed in Table I. From the results, one can see that the correcting coefficients $1/(1-3/2f)$ fall in a narrow range between 1.12 and 1.21. Hence, by eliminating the effects of pores, the thermal conductivity of the nanocomposites still exhibit the same trend with regard to the effects of the nanoparticles contents, i.e., the thermal conductivity decrease with increasing amount of nanosized particles. We can safely reach the conclusion that the introduced nanosized particles are the main contributor for the observed reduction in thermal conductivity of our nanocomposite samples.

With the electrical resistivity, Seebeck coefficient, and thermal conductivity results, the dimensionless figure of merit $ZT$ values for the samples are calculated and presented in Fig. 8. The highest $ZT$ value reaches 0.092 at about 400 °C for sample nano-10%. Compared to the sample bulk, whose highest $ZT$ value is 0.047, the value has nearly doubled. The decrease in the electrical resistivity of the nanocomposites is the most important contributor to the improvement in electrical property even though the improvement is slightly counteracted by the decrease in the Seebeck coefficient. Meanwhile, the inclusion of $CoSb_3$ nanosized particle in a micron-sized $CoSb_3$ matrix results in a reduction in the lattice thermal conductivity. Hence, due to the improvement in both the electrical and thermal properties, the $ZT$ values of the nanocomposites are nearly doubled. These results are very exciting because it shows that nanocomposite approach can be an effective way to increase the figure of merit $ZT$ value not only by decreasing the thermal conductivity, the electrical resistivity can also be decreased too.

## IV. CONCLUSIONS

In summary, the pure $CoSb_3$ nanocomposites with inclusions of $CoSb_3$ nanosized particles in a micron-sized $CoSb_3$ matrix have been prepared. The results for the thermoelectric properties were promising due to the significant reduction in both the electrical resistivity and thermal conductivity. The highest $ZT$ value of 0.092 was obtained at about 400 °C for sample nano-10% nanocomposite. This value is nearly twice that obtained for the sample bulk obtained from micron-sized particles.

[1] F. E. Jaumot, Proc. IRE **46**, 538 (1958).
[2] D. M. Rowe, Renewable Energy **5**, 1470 (1994).
[3] D. M. Rowe, *Thermoelectrics Handbook: Macro to Nano* (CRC, Boca Raton/Taylor & Francis, London, 2006).
[4] T. Caillat, J. P. Fleurial, and A. Borshchevsky, 15th International Conference on Thermoelectrics, 1996, p. 100.
[5] G. S. Nolas, D. T. Morelli, and T. M. Tritt, Annu. Rev. Mater. Res. **29**, 89 (1999).
[6] M. S. Toprak, C. Stiewe, D. Platzek, S. Williams, L. Bertini, E. C. Muller, C. Gatti, Y. Zhang, M. Rowe, and M. Muhammed, Adv. Funct. Mater. **14**, 1189 (2004).
[7] W. Kim, J. Zide, A. Gossard, D. Klenov, S. Stemmer, A. Shakouri, and A. Majumdar, Phys. Rev. Lett. **96**, 045901 (2006).
[8] B. C. Sales, Int. J. Appl. Ceram. Technol. **4**, 291 (2007).
[9] B. Zhang, J. He, X. Ji, M. T. Terry, and K. Amar, Appl. Phys. Lett. **89**, 163114 (2006).
[10] X. B. Zhao, X. H. Ji, Y. H. Zhang, T. J. Zhu, J. P. Tu, and X. B. Zhang, Appl. Phys. Lett. **86**, 062111 (2005).
[11] X. Y. Zhao, X. Shi, L. D. Chen, W. Q. Zhang, S. Q. Bai, Y. Z. Pei, X. Y. Li, and T. Goto, Appl. Phys. Lett. **89**, 092121 (2006).
[12] S. Katsuyama, Y. Kanayama, M. Ito, K. Majima, and H. Nagai, J. Appl. Phys. **88**, 3484 (2000).
[13] J. L. Mi, X. B. Zhao, T. J. Zhu, and J. P. Tu, Appl. Phys. Lett. **91**, 172116 (2007).
[14] L. Yang, H. H. Hng, H. Cheng, T. Sun, and J. Ma, Mater. Lett. **62**, 2483 (2008).
[15] W. S. Liu, B. P. Zhang, J. F. Li, and L. D. Zhao, J. Phys. D: Appl. Phys. **40**, 6784 (2007).
[16] G. J. Snyder and E. S. Toberer, Nature Mater. **7**, 105 (2008).
[17] Z. M. He, C. Stiewe, D. Platzek, G. Karpinski, and E. Muller, J. Appl. Phys. **101**, 043707 (2007).